The Journal of Chemical Physics

Nudged elastic band method for solid-solid transition under finite deformation

Cite as: J. Chem. Phys. **151**, 054110 (2019); https://doi.org/10.1063/1.5113716
Submitted: 06 June 2019 . Accepted: 19 July 2019 . Published Online: 06 August 2019

Arman Ghasemi, Penghao Xiao, and Wei Gao

The Journal of Chemical Physics ARTICLE scitation.org/journal/jcp

Nudged elastic band method for solid-solid transition under finite deformation

Cite as: J. Chem. Phys. 151, 054110 (2019); doi: 10.1063/1.5113716
Submitted: 6 June 2019 • Accepted: 19 July 2019 •
Published Online: 6 August 2019

Arman Ghasemi,[1] Penghao Xiao,[2] and Wei Gao[1,a)]

AFFILIATIONS

[1] Department of Mechanical Engineering, The University of Texas at San Antonio, San Antonio, Texas 78249, USA
[2] Materials Science Division, Lawrence Livermore National Laboratory, Livermore, California 94550, USA

[a)] **Electronic mail:** wei.gao@utsa.edu

ABSTRACT

Solid-state nudged elastic band (SSNEB) methods can be used for finding solid-solid transition paths when solids are subjected to external stress fields. However, previous SSNEB methods may lead to inaccurate barriers and deviated reaction paths for transitions under stress and finite deformation due to an inaccurate evaluation of the external work contributions in enthalpies. In this paper, a finite deformation nudged elastic band (FD-NEB) method is formulated for finding transition paths of solids under finite deformation. Applications of FD-NEB to a phase transition of silicon from the diamond phase to the β-tin phase under uniaxial compression are presented. The results are compared with those from the generalized solid-state nudged elastic band method.

I. INTRODUCTION

The Nudged Elastic Band (NEB) method is a widely used transition state search method for finding transition paths and barriers. The barriers can then be used to calculate chemical reaction or transition rates within the transition state theory in the harmonic approximation.[1] The transition paths reveal atomic scale mechanisms during transition. Given the initial and final states of a transition process, the NEB converges to a minimum energy path (MEP), i.e., the most probable transition path. The NEB method has been applied to study a wide range of problems such as materials phase transitions,[2,3] dislocation motions,[4,5] fracture formations,[6] surface diffusion,[7] and so on.

The NEB method was first proposed in the mid-1990s[8,9] and since then there have been a number of improvements. One important improvement is to generalize the method for studying transitions of solid-state materials. The conventional NEB only takes atomic positions as transition variables, while the lattice geometries are not adjustable in the optimization process. Hence, it cannot be directly applied to study solid-solid transitions where lattice deformation and external stress fields also contribute to the MEP. To this end, solid-state NEB methods were proposed to include the influence of lattice deformation. Trinkle *et al.* coupled the conventional NEB with a full relaxation on the lattice cell.[10] By contrast, Caspersen and Carter used the NEB exclusively for the lattice cell while always relaxing the atomic positions (a rapid-nuclear-motion approximation).[11] Noting that these two approaches are only appropriate for mechanisms dominated by either atomic or lattice changes, Sheppard *et al.* proposed a generalized solid-state nudged elastic band (G-SSNEB) method,[12] which treats the atomic and lattice variables on equal footing so that transitions involving changes in any combination of degrees of freedom are properly described. Similar to the concept of G-SSNEB, Qian *et al.* developed a variable cell nudged elastic band (VC-NEB) method in which force vectors are the derivatives of the enthalpy surface under hydrostatic pressure with respect to both strain and atomic positions.[13]

We note that, when a stressed solid undergoes finite deformation during transition, the barriers evaluated from these methods may not be accurate depending on the choice of stress and deformation measurements. In this paper, a finite deformation nudged elastic band (FD-NEB) method is proposed based on the concept of G-SSNEB for determining the MEP of solid-state materials under finite deformation. The remainder of the paper is organized as follows. To provide readers a basic background, we first summarize the principles of NEB and G-SSNEB methods and then discuss the

limitations for studying finite deformation. After that, the FD-NEB method is formulated by adding finite deformation variables to the framework of the G-SSNEB method. Finally, an example on stress dependent phase transitions of silicon from the diamond phase to the β-tin phase is used to demonstrate the application of the FD-NEB method.

II. NEB/G-SSNEB AND LIMITATIONS

A. NEB method

In a NEB calculation, a band is initially constructed by connecting a number of intermediate states between the given initial and final states with elastic springs. These intermediate states are usually generated by a linear interpolation between the initial and the final as an initial guess. The task of finding the MEP is then transferred to minimizing the total energy of the elastic band. The "nudged" part is to avoid the deviation of the elastic band from the MEP due to the spring force when the path is curved, the so-called "corner cutting" problem.

For a system containing N atoms, each state on the elastic band has $3N$ degrees of freedom, so the configuration space of each state is described by a $3N$-dimension vector $\boldsymbol{R} = (\boldsymbol{r}_1, \boldsymbol{r}_2, \ldots, \boldsymbol{r}_N)$, where $\boldsymbol{r}$ represents atomic positions. Note that none of the intermediate states are in equilibrium, so they are subjected to the *potential forces* coming from the gradient of the potential energy,

$$\boldsymbol{f}^i_{\text{pot}} = -\nabla \mathcal{V}(\boldsymbol{R}^i), \tag{1}$$

which is a $3N$-dimension force vector, evaluated directly from atomistic calculations (either through empirical potentials or first-principles methods). The superscript i represents ith state along the elastic band. Just minimizing these forces would of course only move the intermediate states into one of the local energy minima, and thus would not help to find the MEP. Therefore, in order to keep the intermediate states evenly spaced on the elastic band, *spring forces* are applied between adjacent states, which are also $3N$-dimension force vectors. To avoid "corner cutting" and the sensitivity of selecting spring constant values for convergence, only certain components of the forces are used in minimizing the band energy. Specifically, the *total force* of an intermediate state i is

$$\boldsymbol{f}^i = \boldsymbol{f}^i_{\text{pot}}\big|_\perp + \boldsymbol{f}^i_{\text{spr}}\big|_\parallel, \tag{2}$$

where $\boldsymbol{f}^i_{\text{pot}}\big|_\perp$ is the potential force perpendicular to the elastic band and $\boldsymbol{f}^i_{\text{spr}}\big|_\parallel$ is the spring force parallel to the band. The tangent vector of the elastic band at each state is defined as the geometry change from its higher-energy neighbor.[14] The total force calculated by Eq. (2) is used to drive the elastic band to the MEP by force-based optimization algorithms.[15] The optimization converges when the total force is reduced to zero. Then, the exact transition state or saddle point (the highest energy point along the MEP) can be obtained with the climbing image method.[16]

B. Solid-state NEB method

The degrees of freedom in the NEB described above are usually atomic positions only, and the geometry of the supercell is not adjustable during the search of the MEP. The solid-state NEB method generalizes the atomic configurational space by adding lattice degrees of freedom. Consider a crystal lattice subjected to a constant *Cauchy stress* tensor $\boldsymbol{\sigma}_{\text{app}}$. Due to lattice deformation, an *internal restoring stress* $\boldsymbol{\sigma}^i_{\text{cell}}$ is generated inside the lattice cell, which can be evaluated directly from atomistic calculations. At equilibrium conditions, the applied stress $\boldsymbol{\sigma}_{\text{app}}$ equals to the restoring stress $\boldsymbol{\sigma}^i_{\text{cell}}$. However, the intermediate states on the elastic band are not in equilibrium during the transition process, so $\boldsymbol{\sigma}^i_{\text{cell}} \neq \boldsymbol{\sigma}_{\text{app}}$ on these states. Similar to the NEB, springs have to be prescribed between neighboring states. The *resultant spring stress* is represented by $\boldsymbol{\sigma}^i_{\text{spr}}$. Then, the *total stress* acting on the lattice of the intermediate state i is

$$\boldsymbol{\sigma}^i = (\boldsymbol{\sigma}_{\text{app}} - \boldsymbol{\sigma}^i_{\text{cell}})\big|_\perp + \boldsymbol{\sigma}^i_{\text{spr}}\big|_\parallel. \tag{3}$$

In G-SSNEB, the atomic and cell variables have been treated on an equal footing. To achieve this, $\boldsymbol{\sigma}_{\text{app}} - \boldsymbol{\sigma}^i_{\text{cell}}$ and $\boldsymbol{\sigma}^i_{\text{spr}}$ are, respectively, vectorized and combined with $\boldsymbol{f}^i_{\text{pot}}$ and $\boldsymbol{f}^i_{\text{spr}}$ in Eq. (2) to form a *generalized force vector*, which are then projected in the directions perpendicular and parallel to the elastic band. To achieve better convergence, a scaling factor is applied to the stresses to ensure their magnitudes scale similarly as the atomic forces.[12]

The atomic positions and cell geometries are simultaneously updated by the generalized force vector until the MEP is converged. Finally, the transition barrier ($\Pi^{\neq}$) is calculated by the enthalpy difference between the initial and transition states,

$$\Pi^{\neq}(\boldsymbol{\sigma}_{\text{app}}) = \mathcal{V}^{\neq}(\boldsymbol{\sigma}_{\text{app}}) - V_0 \boldsymbol{\sigma}_{\text{app}} : \boldsymbol{\epsilon}^{(\text{t})}, \tag{4}$$

where $\mathcal{V}^{\neq}$ is the potential energy difference between transition and initial states, V_0 is the volume of the initial lattice, and $\boldsymbol{\epsilon}^{(\text{t})}$ is the strain tensor at the transition state with respect to the initial state. The symbol ":" represents the inner product (i.e., a double contraction) of second order tensors. It should be noted that the strain defined in G-SSNEB is different from the conventional strains used in mechanics (see discussions in Sec. III A).

C. Limitation for finite deformation

In G-SSNEB, stress is measured by the Cauchy stress, which is *(force in current state)/(area in current state)* by definition. As a known fact in continuum mechanics, Cauchy stress is not a work conjugate to any kind of strain, including the strain defined in G-SSNEB. Therefore, the inner product in Eq. (4) is *ill-defined* and does not yield correct work done by external stress under finite deformation.

This can be simply illustrated by an example shown in Fig. 1, where a cubic crystal undergoes phase transition when it is subjected to a constant compressive Cauchy stress σ_{app}. Due to the Poisson effect, the cross section area increases upon compression, so the applied total force, calculated by $\sigma_{app}A$, also increases during transition. Hence, the work done by this varying force has to be calculated by an integration given the force-displacement relationship (which is usually not a prior knowledge for transition). The work calculated from Eq. (4), denoted by $\sigma_{app}A_0(l - l_0)$, can only serve as an approximation for small deformation when $A \approx A_0$.

Indeed, in a laboratory, it is the applied force that is easily controlled not the Cauchy stress due to the difficulty of tracking the

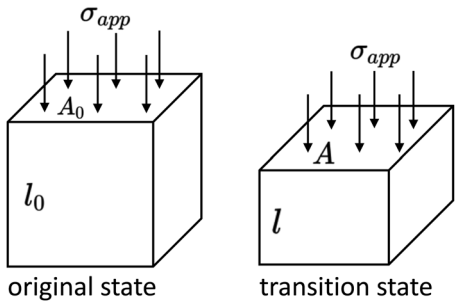

FIG. 1. Phase transition of a cubic crystal under a constant compressive Cauchy stress.

deformed area. Therefore, other types of stresses, such as the first or second *Piola-Kirchhoff (P-K) stress* (detailed discussion on these stresses is in Sec. III A) are also used in mechanics for finite deformation. For example, the *first P-K stress*, denoted by a second order tensor **P**, is the *(force in current state)/(area in reference state)*.[17] Based on this definition, when the applied force is constant, the stress **P** also stays constant. In the previous example, if **P** is used as a control variable for searching the MEP, the work can then be correctly calculated as $P_{app}A_0(l - l_0)$.

Assuming that the applied Cauchy stress stays constant during the transition process, is it possible to evaluate the correct work with Cauchy stress? In this case, the power done by Cauchy stress per unit volume is $\boldsymbol{\sigma} : \dot{\boldsymbol{\epsilon}}$ where $\dot{\boldsymbol{\epsilon}}$ is the rate of a small strain tensor (which is called the power conjugate of Cauchy stress);[17] therefore, the work could be calculated by an integration of the power along the deformation path. However, it is practically difficult to get an integrable deformation path in NEB calculation. More importantly, the work calculated by integration may become path dependent and thus nonphysical. Therefore, it is challenging to get the exact value of barriers under constant Cauchy stress due to the difficulty of evaluating correct external work, making it difficult to quantify the error of G-SSNEB for transitions under finite deformation. There is a special case, the *hydrostatic* compression, where the Cauchy stress (the pressure p) is constant. In this case, the work is simply $p\Delta V$ where ΔV is the volume change. It is worth pointing out that Eq. (4) only provides a first-order approximation of the work term for small deformations in this case. For example, when a cube with unit length is hydrostatically compressed by a unit pressure into a cube with a half of unit length, the correct work should be 7/8 while Eq. (4) yields 3/2.

Depending on the scenarios, it is certainly of interest for researchers to examine their previous results, when Cauchy stress was used for barrier calculations in their studies. First of all, if applied stress is zero, there is no work evaluation so the barrier calculated by G-SSNEB is accurate. When applied stress is not zero, one needs to check the change of the surface area on which the stress is applied. If the change is small and negligible, the barriers calculated by G-SSNEB are acceptable. For example, during a transition under pure shear deformation, if the lattice surface area varies little, G-SSNEB results provide a good approximation even though the lattice shape could be substantially sheared. In addition, as discussed above, the calculations for hydrostatic compression cases (when the volume change between the initial and transition states is large) also require examination if Eq. (4) was used.

When the first or second P-K stress is used for the SSNEB calculation, the lattice deformation should be measured with their work conjugate pairs: deformation gradient or Green-Lagrangian strain. It is important to note that the correction cannot be done by only simply converting $\boldsymbol{\sigma}_{app}$ and $\boldsymbol{\epsilon}^{(t)}$ into the stress and strain of the correct types at the evaluation of work, because the change of the stress type affects the position of the transition state and MEP. Likewise, one cannot simply take the images from G-SSNEB and recalculate the enthalpy using P-K stress. Therefore, a different formulation on the computation method is needed.

III. FD-NEB ALGORITHM

A. Description of finite deformation

A crystal can be modeled by a lattice cell that is replicated by periodic boundary conditions along three lattice vectors $\boldsymbol{h}_1$, $\boldsymbol{h}_2$, and $\boldsymbol{h}_3$. Then, the cell geometry can be described by a cell matrix $\mathbf{H} = [\boldsymbol{h}_1\, \boldsymbol{h}_2\, \boldsymbol{h}_3]$. Like in G-SSNEB, we can further confine $\boldsymbol{h}_1$ and $\boldsymbol{h}_2$, respectively, to axis-1 and plane 1–2, as shown in Fig. 2. In this way, the rotational degrees of freedom of the lattice are eliminated and **H** only includes 6 independent variables,

$$\mathbf{H} = \begin{bmatrix} H_{11} & H_{21} & H_{31} \\ 0 & H_{22} & H_{32} \\ 0 & 0 & H_{33} \end{bmatrix}. \tag{5}$$

The change of the nonzero component H_{ij} can be considered as the kinematics resulting from the corresponding σ_{ij} acting on the cell, which is defined in Eq. (3). This feature has been used in G-SSNEB for stress based cell optimization.

To describe finite deformation, a reference state has to be specified so that deformation and stress can be evaluated based on this state. While there are no restrictions on choosing the reference state, for convenience, we select the *initial state under zero stress* as the reference state in FD-NEB calculations. The lattice vectors and cell matrix of this reference state are represented by $\boldsymbol{h}_\alpha^0 (\alpha = 1, 2, 3)$ and $\mathbf{H}^0$. For an arbitrary state i on the elastic band, the lattice vectors and cell matrix are represented by $\boldsymbol{h}_\alpha^i$ and $\mathbf{H}^i$. Under a homogeneous finite deformation, $\boldsymbol{h}_\alpha^0$ can be mapped to $\boldsymbol{h}_\alpha^i$ by a second order *deformation gradient* tensor **F**,

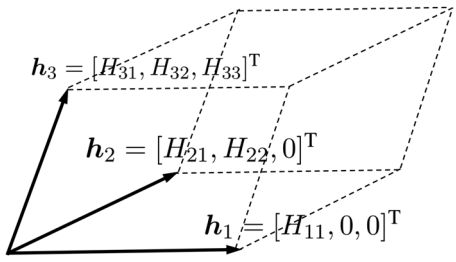

FIG. 2. Schematic of the lattice cell used in FD-NEB calculation, defined by 3 lattice vectors.

$$\boldsymbol{h}_\alpha^i = \mathbf{F}^i \boldsymbol{h}_\alpha^0, \tag{6}$$

where $\mathbf{F}^i$ represents a finite deformation mapping of state i. Using the cell matrix, $\mathbf{F}^i$ can be written as

$$\mathbf{F}^i = (\mathbf{H}^i)(\mathbf{H}^0)^{-1}. \tag{7}$$

The work conjugate of $\mathbf{F}$ is the first P-K stress $\mathbf{P}$, which is related to the Cauchy stress by

$$\mathbf{P} = J\boldsymbol{\sigma}\mathbf{F}^{-\mathrm{T}}, \tag{8}$$

where $J = \det\mathbf{F}$ is the Jacobian of the deformation gradient. The inner product $V_0\mathbf{P}:(\mathbf{F} - \mathbf{I})$ provides the correct work done by a constant stress $\mathbf{P}$ under finite deformation, where the identity tensor represents the undeformed state. Therefore, $\mathbf{F}$ and $\mathbf{P}$ can be taken as control variables in FD-NEB. As discussed in Sec. II C, one advantage of using $\mathbf{P}$ is that it can be directly controlled and measured in some experiments when the applied force is known.

In continuum mechanics,[17,18] another commonly used work conjugate pair is the *second P-K stress* tensor ($\mathbf{S}$) and the *Green-Lagrangian strain* tensor ($\mathbf{E}$), which are defined by

$$\mathbf{S} = J(\mathbf{F})^{-1}\boldsymbol{\sigma}(\mathbf{F})^{-\mathrm{T}} \tag{9}$$

and

$$\mathbf{E} = \frac{1}{2}\left[(\mathbf{F})^{\mathrm{T}}\mathbf{F} - \mathbf{I}\right]. \tag{10}$$

The second P-K stress is conceptually defined by *(force in reference state)/(area in reference state)*, a tensor entirely defined in the reference configuration, so it does not have a direct physical interpretation. However, the second P-K stress has mathematical advantages for many theoretical formulations such as describing materials constitutive behavior. Therefore, it could be useful if one wants to integrate FD-NEB calculation to higher level thermodynamic modeling methods in which the second P-K stress is needed.

It is noted that, in G-SSNEB, the strain is defined as $\boldsymbol{\epsilon} = \mathbf{H}^{\mathrm{def}}\mathbf{H}^{-1} - \mathbf{I}$, where $\mathbf{H}^{\mathrm{def}}$ is for the deformed cell. Therefore, G-SSNEB actually uses the deformation gradient ($\mathbf{H}^{\mathrm{def}}\mathbf{H}^{-1}$) instead of the conventional strains to measure the deformation.

B. Add P-K stress to MEP search

In FD-NEB, the finite deformation variables defined above are used for finding MEPs and computing transition barriers. There are two possible ways to do this. The first way is to convert the restoring stress (obtained from atomistic calculations, so the Cauchy stress) into P-K stress, which can be combined with the prescribed P-K stress and spring stress to form a new total P-K stress. Then, the cell optimization can be done with this total P-K stress. Instead of this way, we take another approach which requires minimum modification to G-SSNEB. For each state on the elastic band, the prescribed P-K stress is converted to a Cauchy stress based on Eq. (8) or (9). For example, if the first P-K stress is used, the prescribed Cauchy stress on state i is calculated as

$$\boldsymbol{\sigma}_{\mathrm{app}}^i = \frac{1}{J}\mathbf{P}_{\mathrm{app}}(\mathbf{F}^i)^{\mathrm{T}}, \tag{11}$$

where $\mathbf{P}_{\mathrm{app}}$ is the applied first P-K stress. In this way, the cell optimization is always controlled by the total Cauchy stress. The same spring stress and scaling factors used in G-SSNEB can be applied here.

After the MEP is obtained based on the modified stress, the transition barrier is calculated as

$$\Pi^{\neq}(\mathbf{P}_{\mathrm{app}}) = \mathcal{V}^{\neq}(\mathbf{P}_{\mathrm{app}}) - V_0\mathbf{P}_{\mathrm{app}} : (\mathbf{F}^{(\mathrm{t})} - \mathbf{F}^{(\mathrm{o})}), \tag{12}$$

where $\mathcal{V}^{\neq}$ is the potential energy difference between transition and initial states, $\mathbf{F}^{(\mathrm{t})}$ and $\mathbf{F}^{(\mathrm{o})}$ are, respectively, the deformation gradients of transition and initial states under stress $\mathbf{P}_{\mathrm{app}}$ with respect to the reference state (whose volume is V_0). To use the second P-K stress, one just needs to replace $\mathbf{P}_{\mathrm{app}}$ and $\mathbf{F}$ in Eq. (12), respectively, with $\mathbf{S}_{\mathrm{app}}$ and $\mathbf{E}$.

Before running FD-NEB, the lattice and atomic positions at both the initial and final states have to be relaxed under the target stress $\mathbf{P}_{\mathrm{app}}$ by using any force-based optimization such as the damped dynamics algorithm. Similar to what is applied in FD-NEB, $\mathbf{P}_{\mathrm{app}}$ is first converted to $\boldsymbol{\sigma}_{\mathrm{app}}$. Then, the residual stress $\boldsymbol{\sigma} = \boldsymbol{\sigma}_{\mathrm{app}} - \boldsymbol{\sigma}_{\mathrm{cell}}$ together with the atomic forces can be gradually reduced to zero by adjusting the structure geometry such that the lattice can be optimized to the target stress $\mathbf{P}_{\mathrm{app}}$.

C. Implementation of FD-NEB

FD-NEB is implemented based on the Atomic Simulation Environment (ASE), an open source Python package which has also been used for G-SSNEB. The advantage of using ASE is that it provides an interface to various external atomistic computational codes, such as Vienna *Ab initio* Simulation Package (VASP) and LAMMPS. ASE can create an "atom object" that has information about the potential energy, atomic positions and forces, lattice geometry, and Cauchy stress. These atomic attributes will be read by FD-NEB for calculating the total forces and stresses defined above. Finally, the calculated forces and stresses will be passed to a force-based optimization algorithm for updating atomic positions and lattice vectors. The FD-NEB computation code is developed based on the G-SSNEB code. It is implemented based on an open source project Transition State Library for ASE (TSASE).

IV. EXAMPLE: PHASE TRANSITION OF SILICON UNDER STRESS

The phase transition of silicon is used to demonstrate the application of FD-NEB for solid-solid transition under external stress fields. Under ambient conditions, the most stable phase of Si is a diamond structure. Under compressive stress, Si undergoes a first order phase transition from the diamond structure (Si-I) to the metallic β-tin structure (Si-II). With further increase of compression, Si continuously exhibits many other different phases. Releasing loads does not lead to a recovery of the initial Si-I phase but instead to a series of metastable phases.[19] Therefore, phase transition of Si is a rather complicated process, and there are still many unknowns despite decades of research on both experimental[20–22] and theoretical[23–26] sides. Particularly, we have not found any transition state calculations on Si to show how external stress changes the phase transition barriers.

Here, we focus on the transition from Si-I to Si-II on a pristine Si structure. Meanwhile, the transition under uniaxial compression is considered. An important feature of this phase transition is that the Si lattice is deformed up to 35% (measured between initial and transition states) and hence a finite deformation problem.

The energy, interatomic force, and stress were evaluated from the density functional theory (DFT). All the DFT calculations in this study were performed using the plane-wave-based Vienna *Ab initio* Simulation Package (VASP[27,28]). Electron exchange and correlation energies were calculated with the generalized gradient approximation using the Perdew–Burke–Ernzerhof (PBE) functional.[29] The projector augmented wave (PAW) method[30,31] was used to represent ionic cores, and the kinetic energy cutoff for the plane-wave basis describing the valence electrons was set to 319 eV. A 6 × 6 × 6 k-point mesh was used to sample the Brillouin zone.

The atomic structure of Si used in this study at different phases is shown as the inserted images in Fig. 3(a). The supercell contains 8 atoms. At zero stress, there is no work evaluation in the MEP calculation, so FD-NEB yields the same results as G-SSNEB, as shown in Fig. 3(a). The reaction coordinate primarily involves lattice degrees of freedom. When a constant load is applied, the first P-K stress stays constant throughout the transition process while the Cauchy stress varies. If one disregards this practical loading constrains, second P-K stress can also be used legitimately. Although the Cauchy stress leads to ill-defined and incorrect enthalpy evaluations, the calculations with both the Cauchy and P-K stresses are conducted at different stress levels for comparison. The typical MEP is shown in Fig. 3(b) for a 10 GPa uniaxial stress. It is not surprising that different stress representations not only lead to different barriers but also different paths. This difference becomes more significant with increasing applied stress, demonstrated by the variation of barriers with stress in Fig. 4. It is noted that the barrier disappears when the applied Cauchy stress is beyond 12 GPa, which means that the transition could occur in this case without any thermal activation.

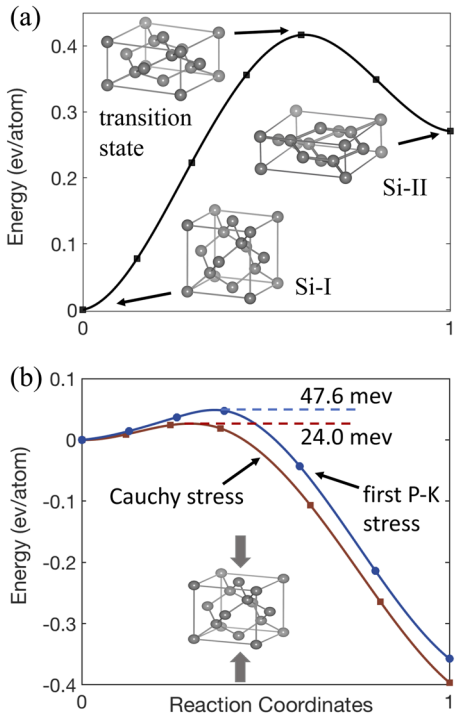

FIG. 3. (a) Zero stress MEP. The inserted images show atomic structures of Si-I (5.47 Å × 5.47 Å × 5.47 Å), Si-II (6.92 Å × 6.92 Å × 2.55 Å), and transition state (6.35 Å × 6.35 Å × 3.45 Å). (b) Comparison of MEPs calculated by using Cauchy stress (with G-SSNEB) and first P-K stress (with FD-NEB) at 10 GPa compressive stress. MEPs are fitted with splines.

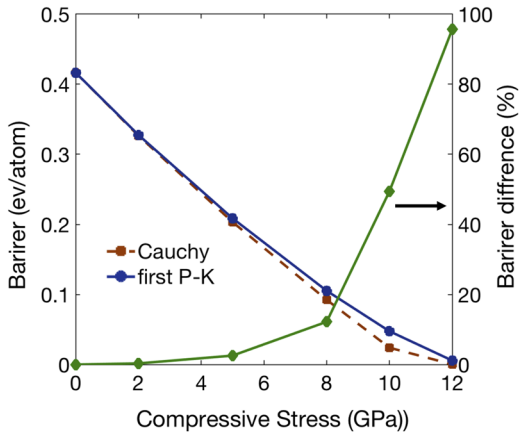

FIG. 4. Barriers as a function of applied stress. The differences are calculated by $(\Pi^{\pm}_{\text{Cauchy}} - \Pi^{\pm}_{\text{PK}})/\Pi^{\pm}_{\text{PK}}$.

The transition pathway calculated with the Cauchy stress is qualitatively similar to the ones calculated with P-K stress in this example. However, it may not be the case for other material systems. If two or several (stress sensitive) competing transition mechanisms exist simultaneously, the calculation conducted with the Cauchy stress may lead to a different pathway due to the incorrect evaluation of enthalpy.

V. SUMMARY

Solid-solid transitions are usually accompanied with finite lattice deformation. Accurate evaluation of the transition barriers is critical for computing kinetic rates of the transition. Under applied stresses, the work done by the external load contributes significantly to the barrier height and needs to be evaluated carefully. In this paper, we emphasize that the previous solid-state NEB algorithm may lead to inaccurate barriers and deviated reaction paths when the Cauchy stress is used for work evaluations under finite deformation. The FD-NEB method is formulated by introducing finite deformation variables to the G-SSNEB method and implemented based on facile modifications to the previous algorithm. An example of silicon phase transition is presented to demonstrate the difference brought by the new implementation.

ACKNOWLEDGMENTS

W.G. and A.G. acknowledge the startup fund from the University of Texas at San Antonio (UTSA) and the Grant for Research Advancement and Transformation (GREAT) from the UTSA Office of the Vice President for Research, Economic Development, and Knowledge Enterprise. Part of P.X.'s work was performed under the auspices of the U.S. Department of Energy by Lawrence Livermore National Laboratory under Contract No. DE-AC52-07NA27344. The authors acknowledge the Texas Advanced Computing Center (TACC) at the University of Texas at Austin for providing HPC resources that have contributed to the research results reported within this paper.

REFERENCES

[1] R. A. Olsen, *An Introduction to Transition State Theory* (Winter School Lecture at Han-sur-Lesse, Belgium, 2006).
[2] P. Xiao and G. Henkelman, "Communication: From graphite to diamond: Reaction pathways of the phase transition," J. Chem. Phys. **137**, 101101 (2012).
[3] P. Xiao, J.-G. Cheng, J.-S. Zhou, J. B. Goodenough, and G. Henkelman, "Mechanism of the $CaIrO_3$ post-perovskite phase transition under pressure," Phys. Rev. B **88**, 144102 (2013).
[4] T. Zhu, J. Li, A. Samanta, A. Leach, and K. Gall, "Temperature and strain-rate dependence of surface dislocation nucleation," Phys. Rev. Lett. **100**, 025502 (2008).
[5] R. Ramachandramoorthy, W. Gao, R. Bernal, and H. Espinosa, "High strain rate tensile testing of silver nanowires: Rate-dependent brittle-to-ductile transition," Nano Lett. **16**, 255–263 (2015).
[6] S. Huang, S. Zhang, T. Belytschko, S. S. Terdalkar, and T. Zhu, "Mechanics of nanocrack: Fracture, dislocation emission, and amorphization," J. Mech. Phys. Solids **57**, 840–850 (2009).
[7] M. Villarba and H. Jónsson, "Diffusion mechanisms relevant to metal crystal growth: Pt/Pt (111)," Surf. Sci. **317**, 15–36 (1994).
[8] H. Jónsson, G. Mills, and K. W. Jacobsen, "Nudged elastic band method for finding minimum energy paths of transitions," in *Classical and Quantum Dynamics in Condensed Phase Simulations* (World Scientific, 1998), pp. 385–404.
[9] G. Mills, H. Jónsson, and G. K. Schenter, "Reversible work transition state theory: Application to dissociative adsorption of hydrogen," Surf. Sci. **324**, 305–337 (1995).
[10] D. Trinkle, R. Hennig, S. Srinivasan, D. Hatch, M. Jones, H. Stokes, R. Albers, and J. Wilkins, "New mechanism for the α to ω martensitic transformation in pure titanium," Phys. Rev. Lett. **91**, 025701 (2003).
[11] K. J. Caspersen and E. A. Carter, "Finding transition states for crystalline solid–solid phase transformations," Proc. Natl. Acad. Sci. U. S. A. **102**, 6738–6743 (2005).
[12] D. Sheppard, P. Xiao, W. Chemelewski, D. D. Johnson, and G. Henkelman, "A generalized solid-state nudged elastic band method," J. Chem. Phys. **136**, 074103 (2012).
[13] G.-R. Qian, X. Dong, X.-F. Zhou, Y. Tian, A. R. Oganov, and H.-T. Wang, "Variable cell nudged elastic band method for studying solid–solid structural phase transitions," Comput. Phys. Commun. **184**, 2111–2118 (2013).
[14] G. Henkelman and H. Jónsson, "Improved tangent estimate in the nudged elastic band method for finding minimum energy paths and saddle points," J. Chem. Phys. **113**, 9978–9985 (2000).
[15] D. Sheppard, R. Terrell, and G. Henkelman, "Optimization methods for finding minimum energy paths," J. Chem. Phys. **128**, 134106 (2008).
[16] G. Henkelman, B. P. Uberuaga, and H. Jónsson, "A climbing image nudged elastic band method for finding saddle points and minimum energy paths," J. Chem. Phys. **113**, 9901–9904 (2000).
[17] E. B. Tadmor, R. E. Miller, and R. S. Elliott, *Continuum Mechanics and Thermodynamics: From Fundamental Concepts to Governing Equations* (Cambridge University Press, 2012).
[18] E. B. Tadmor and R. E. Miller, *Modeling Materials: Continuum, Atomistic and Multiscale Techniques* (Cambridge University Press, 2011).
[19] S. Wippermann, Y. He, M. Vörös, and G. Galli, "Novel silicon phases and nanostructures for solar energy conversion," Appl. Phys. Rev. **3**, 040807 (2016).
[20] J. Kasper and S. Richards, "The crystal structures of new forms of silicon and germanium," Acta Crystallogr. **17**, 752–755 (1964).
[21] J. Z. Hu, L. D. Merkle, C. S. Menoni, and I. L. Spain, "Crystal data for high-pressure phases of silicon," Phys. Rev. B **34**, 4679 (1986).
[22] Y.-X. Zhao, F. Buehler, J. R. Sites, and I. L. Spain, "New metastable phases of silicon," Solid State Commun. **59**, 679–682 (1986).
[23] A. Mujica, A. Rubio, A. Munoz, and R. Needs, "High-pressure phases of group-IV, III–V, and II–VI compounds," Rev. Mod. Phys. **75**, 863 (2003).
[24] M. Durandurdu, "Diamond to β-sn phase transition of silicon under hydrostatic and nonhydrostatic compressions," J. Phys.: Condens. Matter **20**, 325232 (2008).
[25] V. I. Levitas, H. Chen, and L. Xiong, "Triaxial-stress-induced homogeneous hysteresis-free first-order phase transformations with stable intermediate phases," Phys. Rev. Lett. **118**, 025701 (2017).
[26] N. A. Zarkevich, H. Chen, V. I. Levitas, and D. D. Johnson, "Lattice instability during solid-solid structural transformations under a general applied stress tensor: Example of Si I → Si II with metallization," Phys. Rev. Lett. **121**, 165701 (2018).
[27] G. Kresse and J. Furthmüller, "Efficient iterative schemes for *ab initio* total-energy calculations using a plane-wave basis set," Phys. Rev. B **54**, 11169 (1996).
[28] G. Kresse and J. Hafner, "*Ab initio* molecular dynamics for liquid metals," Phys. Rev. B **47**, 558 (1993).
[29] J. P. Perdew, K. Burke, and M. Ernzerhof, "Generalized gradient approximation made simple," Phys. Rev. Lett. **77**, 3865 (1996).
[30] G. Kresse and D. Joubert, "From ultrasoft pseudopotentials to the projector augmented-wave method," Phys. Rev. B **59**, 1758 (1999).
[31] P. E. Blöchl, "Projector augmented-wave method," Phys. Rev. B **50**, 17953 (1994).